Chapter 1

Introduction

1.1 Background of the remote sensing

Since the 18th century, advances in aerial photography have paved the way for the scientific development of remote sensing. In 1839, Daguerre and Niepce took the first photograph of the Earth's surface. Later, Paris Observatory proposed photography for topological purposes [1]. Around 1858, photos of large regions were taken from balloons. In the 1880s and early 1900s, kites and pigeons were used to transport cameras to altitudes of several hundred meters. With the invention of the airplane, it became possible to collect data over specific areas and under controlled conditions, making aerial photography an extremely important instrument. Towards the end of the 18th century and the beginning of the 19th century, it became apparent that a photograph taken from an incline or building may provide a unique and probably more revealing perspective of a particular landscape. In order to acquire oblique aerial images of the Earth's surface, photographic equipment was mounted on kites, balloons, and aircraft. In 1909, the first aerial photographs were taken from an airplane.

In the mid-1930s, color photography became a reality. At the same time, the creation of films that were sensitive to near-infrared radiation continued. Haze penetration was

enhanced greatly by near-infrared photography. Spectral reflectance qualities of natural topography and the availability of photographic emulsions for aerial color infrared photography were studied extensively during World War II. The primary motivation was to create a new methods for detecting camouflage.

In 1956, Colwell conducted some of the earliest tests on the use of special-purpose aerial photography to categorize and recognize vegetation types and detect diseased and damaged vegetation. National Aeronautics and Space Administration (NASA) sponsored a huge number of studies beginning in the mid-1960s on the application of color infrared and multispectral photography, which led to the launch of multispectral imagers on the Landsat satellites in the 1970s.

Prior to the 1960s, aerial photography was the most used name for remote sensing. During the years 1960 to 2010, the field of remote sensing experienced significant transformations. During the 1960s and 1970s, remote sensing devices were transferred from airborne platforms to space-borne platforms or satellites. NASA supported a large number of programs in the 1960s to investigate the applicability of color infrared and multispectral photography.

During World War II, the development of radars accelerated. Today, the diversity of radar applications is simply astounding. It is utilized to examine ocean surface characteristics, lower and upper-atmospheric phenomena, subsurface and surface land structures, and surface cover. There are numerous types of radar sensor configurations. These include altimeters for topographical measures, scatterometers for surface roughness studies, and polarimetric and interferometric imagers. Midway through the 1950s, significant progress was made in the creation of real-aperture airborne imaging radars. Synthetic-Aperture Radars (SAR), which use coherent signals to obtain high-resolution capabilities from high-flying aircraft, were being developed about the same time. In the mid-1960s, these systems became accessible to the scientific community. Since then, other organizations

have continued to expand the capabilities of radar sensors to examine natural surfaces. This work led to the 1978 orbital flight of the Seasat SAR and the 1981 flight of the Shuttle Imaging Radar (1981, 1984). Several nations have since flown orbital SAR systems.

Beginning in 1986, a new variety of image spectrometer sensors, such as Airborne Visible/Infrared Imaging Spectrometer (AVIRIS), Hyperspectral Imaging Satellite (HySIS), and Hyperion, were created. The number of spectral bands available in this sort of sensing instrument increased from a few to over 200. Over the past two decades, the potential of remote sensing satellites has risen substantially. Observational satellites with a few meters or less spatial resolutions are now available. SAR can now gather images in several bands and polarizations on demand. Satellites are currently obtaining photos of extraterrestrial planets with higher resolutions and more spectral bands. Consequently, with the advancement of remote sensing technology, the scope of applications for monitoring the Earth's surface features more effectively than ever before has expanded across a variety of areas[2, 3].

1.2 Concepts and basis of remote sensing

Remote sensing is the science and art of getting information about a distant object, area, or phenomenon by evaluating data acquired by a sensing device that is not in direct contact with the object, area, or phenomenon being investigated. In several ways, remote data can be acquired using various sensors to obtain information about the distant objects, areas, and phenomena under investigation. The data gathered remotely can occur in many forms, including the distribution of force energy, the distribution of acoustic waves, and the distribution of electromagnetic radiation.

The basis of remote sensing begins with the fundamentals of electromagnetic radiation, how energy interacts with the atmosphere and with the Earth's surface features. Therefore, it is vital to comprehend wave interaction with atmosphere/ionospheric elements, wave

interaction with Earth surface features, and the spectral region limitations imposed by the atmosphere for observing Earth surface characteristics.

1.2.1 Electromagnetic radiation principle

The electromagnetic spectrum is the complete range of wave frequencies that comprise solar radiation. Radio, microwave, infrared, visible, ultraviolet, x-ray, and gamma-ray radiation are the standard divisions of the electromagnetic spectrum, from longest to shortest wavelengths (in μm), as shown in figure 1.1. Only a small portion of the electromagnetic spectrum is visible to humans, which is a limited band of visible light.

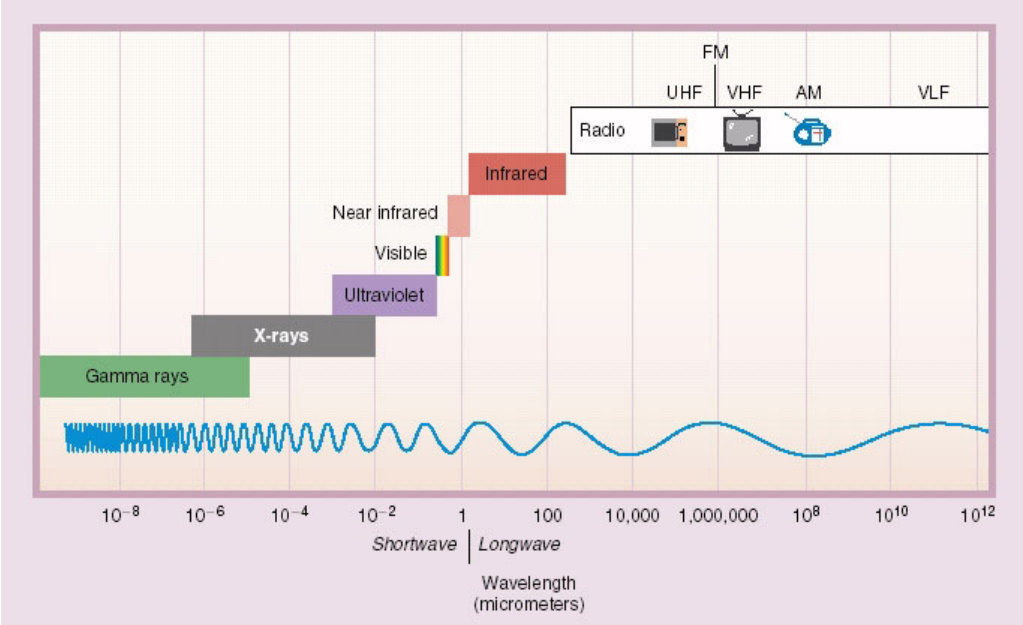

Fig. 1.1 The electromagntic spectrum

Source:cimss.ssec.wisc.edu/satmet/modules/3_em_radiation/emr-2.html

Wavelength (λ), Energy (E), and Frequency (f) are used to characterize electromagnetic waves. Despite each one describing a different aspect of light, they are all mathematically linked. The following two Equations 1.1 and 1.2 illustrate the relationships

between the variables:

$$f = \frac{c}{\lambda} \tag{1.1}$$

$$E = 2\pi\hbar f \tag{1.2}$$

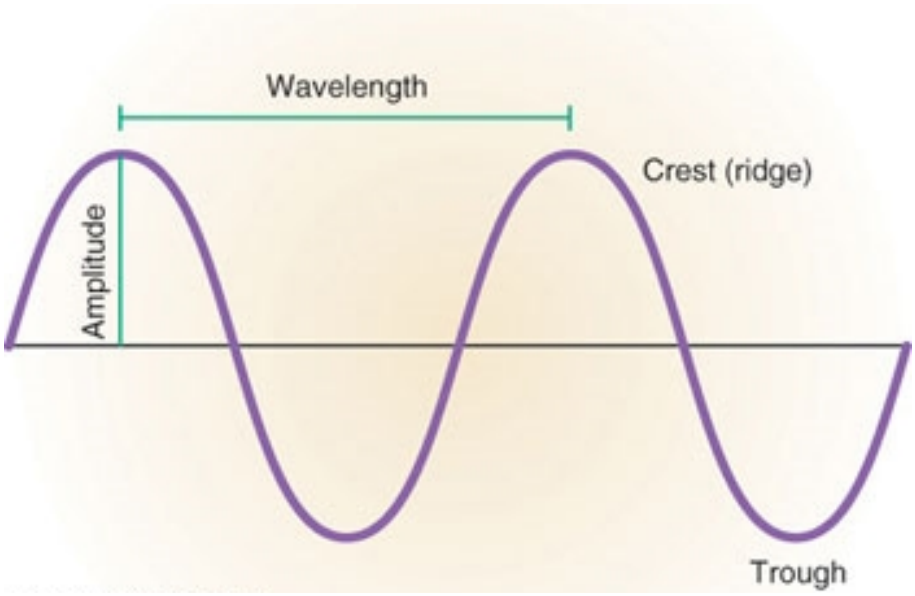

Fig. 1.2 The characteristics of electromagnetic wave

Source: cimss.ssec.wisc.edu/satmet/modules/3_em_radiation/emr-3.html

Where c and $\hbar$ are the Speed of light and reduced Planck's constant. The distance between two consecutive wave crests is the wavelength of an electromagnetic wave, as shown in Figure 1.2. The wave amplitude, which is half the height from the highest point of the crest to the lowest point of the wave, is another attribute that is utilized to describe an electromagnetic wave. It is common practice to express the distance between the tops of waves as a micrometer (abbreviated as μm) or micron. For remote sensing, the sun is the most obvious source of electromagnetic radiation. All matter emits electromagnetic radiation. Specifically, all objects with temperatures above absolute zero temperature ($0K$

or -273°C) emit electromagnetic radiation continually. The mathematical expression of how much energy any object radiates is dependent on the surface temperature of the object and is stated by the Stefan- Boltzmann

$$M = \sigma T^4 \quad (Wm^{-2}) \tag{1.3}$$

Where, M is the amount of radiation emitted by an object per unit surface area of a blackbody in a unit time, σ is Stefan-boltzmann constant ($5.6697\times 10^{-}8\, Wm^{-2}K^{-4}$), and T is the absolute temperture of the object (K).

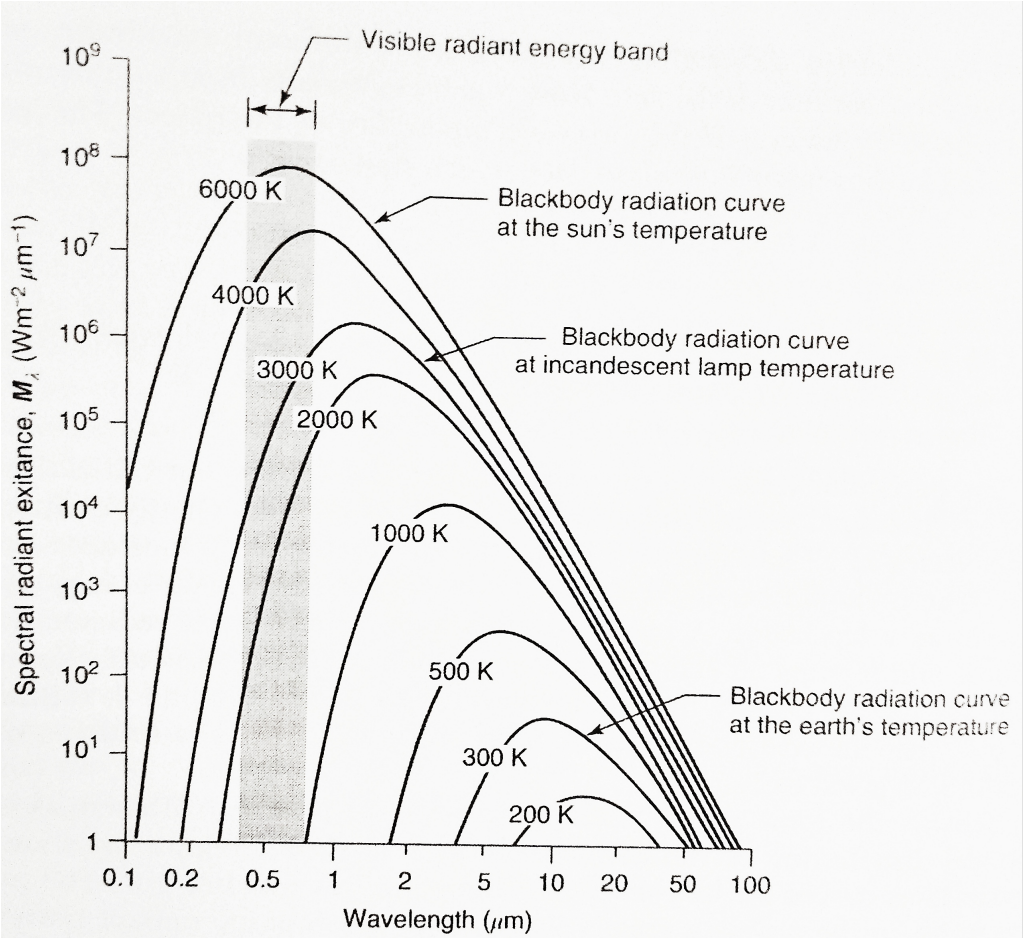

Fig. 1.3 The spectral distribution of energy radiated from blackbodies of various temperatures

Source: [4]

The total energy emitted by an object varies with the temperature, in the same way, the spectral distribution of the emitted energy also varies. Figure 1.3 shows a black body spectral energy distribution curve at a temperature ranging from 200 to 6000K. The unit of spectral radiant exitance on an ordinate scale in the $Wm^{-2}\mu m^{-1}$ express the radiant power coming from the blackbody per $1-\mu m$ spectral interval. Figure 1.3 is the graphical illustration of the mathematical expression stated by the Stefans- Boltzmann law. The total amount of radiation emitted by a radiator increases according to its temperature. As temperature increases, the curves also indicate that the peak of blackbody radiation distribution shifts towards shorter wavelengths. The mathematical expression of the wavelength at which radiation distribution curves reaches their maximum is given by Wein and is commonly known as Weins displacement law,

$$\lambda_{max} = \frac{A}{T} \tag{1.4}$$

Where, λ_{max} is the wavelength of maximum spectral radiant exitance (in μm), A is the Weins constant, and T is temperature (K). The sun emits radiation similarly to a 6000K black body radiator. Numerous incandescent bulbs generate radiation characterized by a 3000K blackbody curve. In consequence, incandescent bulbs emit very little blue light and lack the same spectral composition as natural light. The temperature of the Earth's features like soil, water, and plants is around 300K. According to the Weins displacement law, the peak of the spectral radiant exitance from the Earth features exits at a wavelength of roughly 9.7 μm. Because this is a form of terrestrial heat, it is referred to as thermal infrared energy. Although this energy cannot be seen or photographed, it can be detected using thermal devices. Figure 1.3 shows that the sun has a far higher energy peak (0.5 μm) than the Earth's features. The energy of this magnitude and wavelengths is detectable by our eyes and camera sensors. As a result of solar energy reflection, we can see the Earth's features when the sun is present. Some sensors, such as radar systems, generate

their own source of energy to illuminate features of interest. This type of system is defined as an active system. In contrast, the passive systems sense naturally available energy. For instance, the camera utilizing the flash is a form of active system, and the same camera used in sunlight becomes a passive sensor.

1.2.2 Energy interaction in the atmosphere

Regardless of its source, the radiation observed by remote sensors passes through some distance or path length of the atmosphere. The total effect of the atmosphere varies with the amount of energy being received, atmospheric constituents, distance traveled, and wavelength used. Atmospheric particles and gases can principally influence radiation through the phenomena of scattering and absorption.

Scattering

Atmospheric scattering is the unpredictable dispersal of radiation by atmospheric particles. The process by which an atom, molecule, or particle redirects energy is known as scattering.

Types of scattering

✓Rayleigh scattering- atmospheric atom:

The scattering from atmospheric gas and the small molecule was discovered by Rayleigh in 1971. This type of scattering occurs when the size of a particle is smaller than the radiation wavelength. The intensity of the Rayleigh scattered light is inversely proportional to the fourth power of the wavelength. Rayleigh's scattering scattered the radiation equally in all directions. The phenomenon of the Rayleigh scattering is responsible for blue sky and red sunsets.

✓Mie scattering-aerosol:

The Mie scattering occurs when the size of the atmospheric scatterer is equal to the radiation wavelength. The scattering by aerosols such as water vapor, smoke particles, and

fine dust are responsible for Mie scattering. This sort of scattering has a tendency to affect longer wavelengths than Rayleigh's scatter. When there are hazy conditions and bigger particles or gas molecules present in abundance, Mie scattering predominates in the lower sections of the atmosphere. This is also true when there are foggy conditions.

✓**Non-selective scattering- cloud:**

Non-selective scattering occurs when the diameter of the atmospheric scatterer is much larger than the radiation wavelength being sensed. The atmospheric scatterer, such as water droplets, ice crystals, and volcanic ash, is responsible for non-selective scattering. It is referred to as non-selective scattering because all wavelengths are scattered almost equally. Fog and clouds seem white to human eyes because of non-selective selective scattering, like blue, green, and red light are scattered in roughly equal amounts (i.e., $blue + green + red = white$).

Absorption

The atmospheric absorption led to the effective loss of electromagnetic signal to atmospheric constituents compared to the scattering. The most efficient and effective energy absorbers in the atmosphere are carbon dioxide, water vapor, and ozone. These gases have a tendency to absorb particular bands of the electromagnetic spectrum. Consequently, they have a significant impact on the design of any remote sensing system. The spectral regions of the electromagnetic spectrum in which the atmosphere possesses a high degree of transparency are known as 'Atmospheric windows'.

Figure 1.4 (Top) illustrates the spectrum distribution of energy emitted by the sun and by Earth features. Figure 1.4 (Middle) represents the spectral regions of the electromagnetic spectrum with wavelengths appropriate for remote sensing data collecting to exploit earth features. The white region represents the blocked spectral region by atmospheric absorbers. In addition , Figure 1.4 (Bottom) depicts the spectral sensitivity range for various sensors.

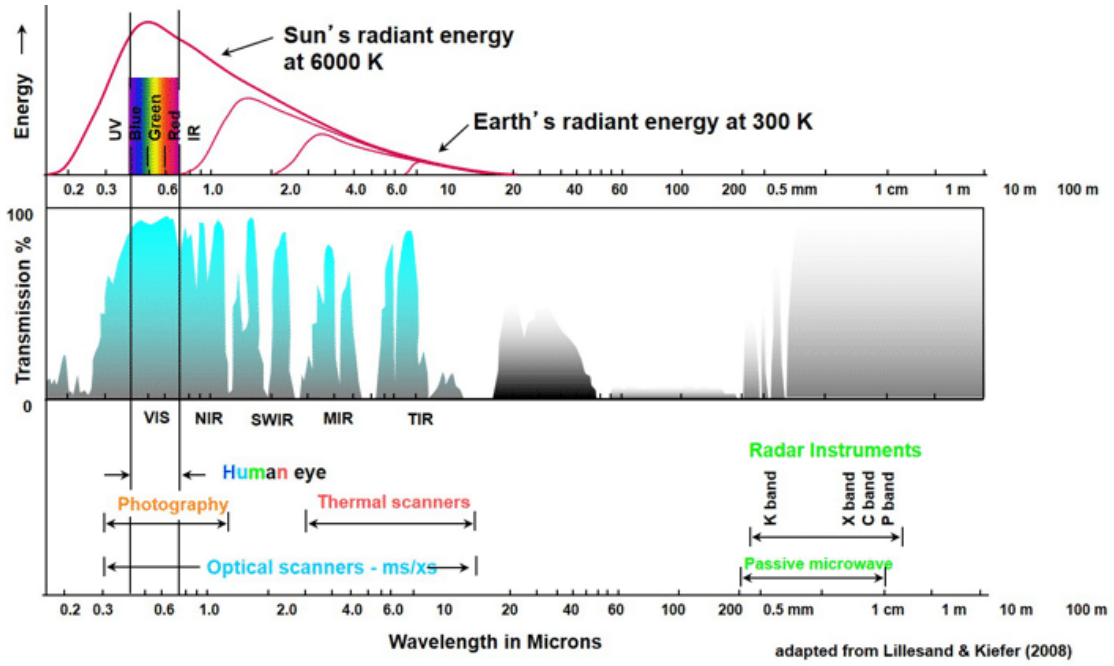

Fig. 1.4 Spectral characteristics of (Top) Energy sources, (Middle) Atmospheric transmittance, and (Bottom) Remote sensing system

Source: [4]

The portion of the electromagnetic spectrum that is most sensitive to human sight, known as the visible spectrum, also coincides with the peak energy value of the spectral distribution of the sun and the atmospheric windows of the visible spectrum. The Earth's surface object gives off heat energy that lines up with atmospheric windows around 3 to 5 μm and 8 to 14 μm in the thermal infrared part of the electromagnetic spectrum. In comparison, the microwave regions (1 mm to 1 m) have a large atmospheric window. The crucial aspects of Figure 1.4 are the interplay and interdependence between the principal sources of electromagnetic energy, atmospheric windows via which source energy can be transported to and from Earth's surface features, and the spectral sensitivity of sensors available to detect and record energy. Therefore, the following points are important in selecting sensors for any given remote sensing application (1) availability of the sensing device in the given spectral region application; (2) whether an atmospheric window for the desired spectral ranges is present or not; (3) the source, magnitude, and spectral distribution of the energy

present in various wavelength bands; and (4) The choice of spectral bands for sensing devices must be based on how energy interacts with the objects under investigation.

1.2.3 Energy interaction with Earth surface features

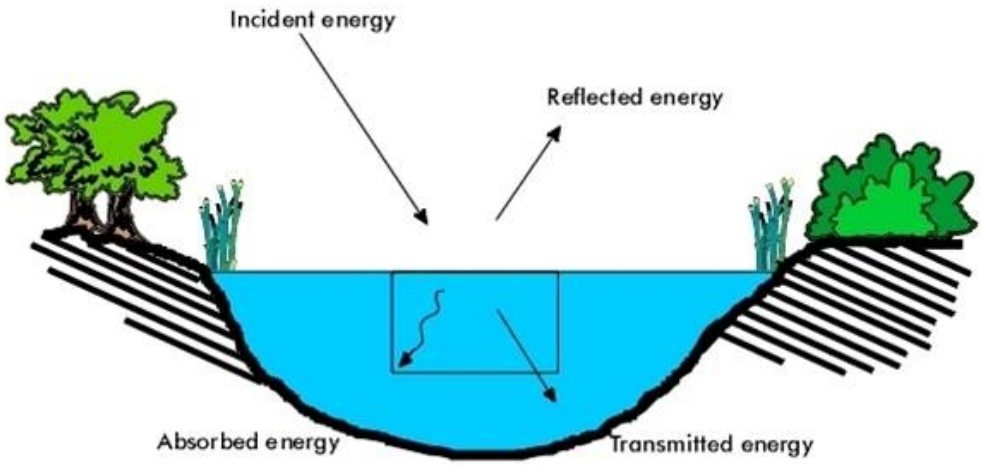

Fig. 1.5 The fundamental interaction between electromagnetic radiation and an Earth surface features

Source: www2.geog.soton.ac.uk/users/trevesr/obs/rseo/energy_interactions_with_the_Earths_surface.html

Three fundamental interactions are possible when the electromagnetic radiation interacts with the Earth's surface features, as shown in Figure 1.5. When the energy wave incident on a water body, a portion of its incident energy is reflected, absorbed, and/or transmitted. Applying the law of conservation of energy, we can say that the total energy dissipated via reflection, transmission, and absorption is equal to incident energy and can be mathematically expressed as

$$E_i(\lambda) = E_r(\lambda) + E_t(\lambda) + E_a(\lambda) \tag{1.5}$$

Where, $E_i(\lambda)$, $E_r(\lambda)$, $E_t(\lambda)$, and $E_a(\lambda)$ are the incident, reflected, transmitted, and absorbed energies, respectively. The reflected, transmiited, and absorbed chracteristics of Earth surface could be quantified in terms of reflectance (ρ_λ), absorptance (α_λ) and transmittance (τ_λ) on dividing Equation 1.5 by incident energy (i.e., $E_i(\lambda)$). Hence, it gives

$$\frac{E_r(\lambda)}{E_i(\lambda)} + \frac{E_t(\lambda)}{E_i(\lambda)} + \frac{E_a(\lambda)}{E_i(\lambda)} = 1 \tag{1.6}$$

$$\rho_\lambda + \alpha_\lambda + \tau_\lambda = 1 \tag{1.7}$$

The characteristics of the surface material and the way it is arranged determine the proportions of the incident radiant energy that is reflected, absorbed, and transmitted, respectively. For instance, interaction at optical and thermal wavelengths takes place primarily through the electric field vector in electromagnetic radiation, which causes electronic and vibrational transitions in the material. When it comes to microwaves, the dipole moment of the material (also known as the dielectric constant) determines how strongly the two things interact with one another. It is essential to keep in mind that these three parameters are also dependent on the wavelength; hence, the proportional amounts of energy that are reflected, absorbed, or transmitted change depending on the wavelength. Thus, it is characterized in terms of spectral response as the values ρ_λ, α_λ, and τ_λ.

1.3 Microwave for remote sensing

As we have discussed the brief history of remote sensing in section 1.1, we learned that microwave remote sensing is a relatively new concept compared to aerial photography. Since the early 1960s, microwaves have been utilized in various civilian applications. The microwave has distinct and unique features that offer a number of advantages to Earth's environment. Microwave is not dependent on the sun. It has its own energy source and can

penetrate the cloud. These unique characteristics provide day-night sensing of the Earth in all-weather circumstances. Figure 1.6 depicts the attenuating effect of clouds, rain, snow, and clean air on the transmission of radio waves between space and the Earth's surface.

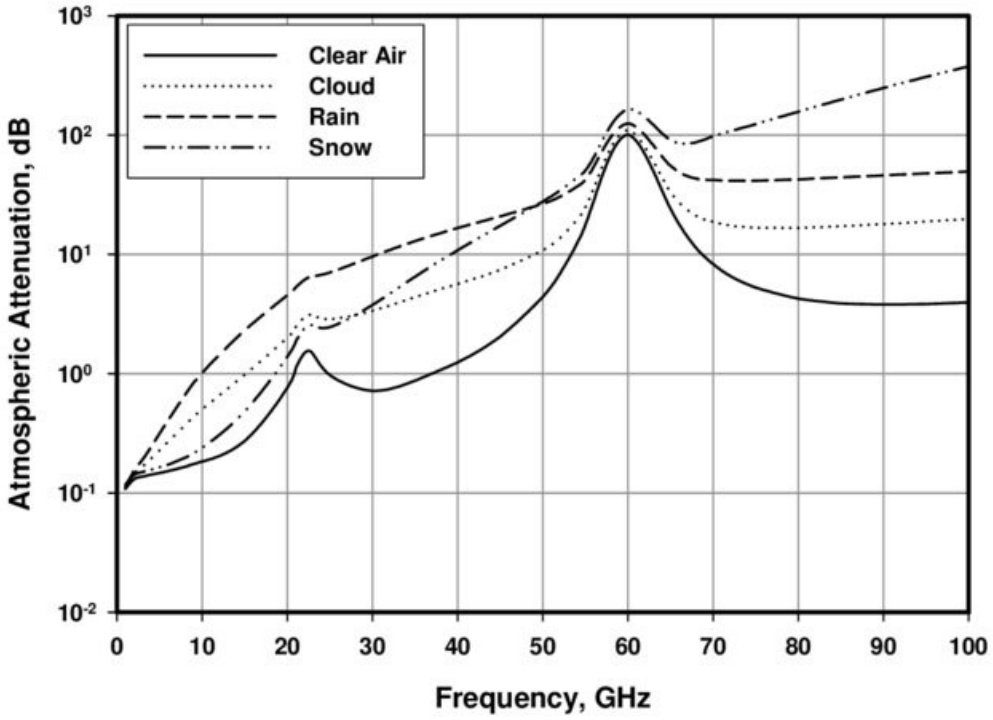

Fig. 1.6 The attenuating effect of clouds, rain, snow, and clean air on the transmission of radio waves between space and the Earth's surface

Source: www.researchgate.net/publication/252761039_The_Effect_of_Earth%27s_Atmosphere_on_Radio-astronomical_Observations/figures

It demonstrates that rain has the most attenuating effect, followed by clouds, snow, and clean air. Microwaves are capable of penetrating deeper into vegetation and even the upper soil surface, which is another significant advantage of their employment. The penetrating ability of the microwave is significantly dependent on the vegetation water content, the density of the vegetation, and microwave frequencies. Lower frequencies can penetrate much deeper compared to the higher frequencies. As a result, the higher frequencies are used to get upper-layer information on the vegetation. In contrast, lower frequencies are

used to yield information on the surface beneath vegetation. The penetrating capability of lower microwave frequencies in dry soil is substantial compared to wet soil. Third, and perhaps most importantly, microwaves provide different information than visible and infrared electromagnetic spectrums. Specifically, the microwave scattering from the Earth's natural target is dependent on the electrical (dielectric) and geometric (structural and roughness) properties of the surface. With the proper sensor design, it is possible to obtain information about the target's electrical and geometrical properties. Thus we can conclude that the microwave-derived properties such as bulk-dielectric, geometric, and molecular resonance complement the data retrieved from visible and infrared radiation.

1.4 Overview of microwave sensor

As shown in Figure, microwave sensors are basically divided into two broad classes: active (i.e., known as radars) and passive (known as radiometers). The only difference is that radars have their own source, including both transmitter and receiver. However, the radiometer relies on reflectance; hence, it only has a receiver. Both the sensors are employed on aircraft and spacecraft to investigate Earth and other planets. These broad classes are further divided into subclasses based on their operational characteristics and functions. The subsequent discussion will focus on our area of interest, the active microwave sensor (i.e., space-borne radar). There are five broad categories of active microwave sensors: SAR, Side-Looking Airborne Radar (SLAR), scatterometers, altimeters, and meteorological radar. Both SAR and SLAR are designed to obtain photographs from a moving platform. SAR uses synthetic-aperture-antenna-processing techniques, as its name suggests, whereas other sensors often use an actual aperture antenna. The Inverse synthetic-aperture radar (ISAR) is used to detect extraterrestrial entities from the ground. This system delivers modulated pulses and constructs backscatter images using doppler/range processing. Although SAR has a substantially higher complexity than other sensors, it offers the highest resolution.

Scatterometers are capable of relatively accurate radar backscatter measurements, but their resolution is often lower than that of SARs. Altimeters are special radars made to measure the height of a platform, but the scattered echo can also be used to retrieve other information. Weather radars are special scatterometers that measure things like rain and weather conditions. Interferometric SAR, also termed InSAR or IFSAR, is a type of SAR used to measure the topography and movement of surfaces. In addition, the information about surveillance radars, which are made to detect ships, planes, and missiles, is detailed in [5] and [6].

1.4.1 Space-borne radars

The space-borne radars were initially developed and used for military purposes. This section will focus on the space-borne radar used for civilian applications. The history of the space-bone microwaves sensor flown for civilian applications is detailed in [7]. In the early 1960s, ideas for SAR for Earth observation were developed, but the first such radar to fly in space was launched aboard the oceanographic satellite Seasat in June 1978 [8]. After that, During the 1980s, 1990s, and early 2000, many shuttle SAR missions were undertaken; notably the Shuttle Radar Topography Mission (SRTM), which employed radar interferometry to survey global surface topography [9]. Scatterometers and altimeters are the other two classes that have been extensively flown aboard spacecraft. However, the scatterometer will be our primary emphasis. The term scatterometer was coined in 1965. It is used for measuring the radar scattering coefficient quantitatively. During World War II, scatterometer coefficient measurements were conducted by [10] and maintained afterward by [11, 12]. Long provides an overview of numerous scattering measurements conducted before 1975 [13].

In 1974, the S-193 scatterometer was flown onboard Skylab to measure the scattering from space. It established radar's capacity to estimate near-surface wind speed from outer

space [14]. This experiment's success led to the 1978 launch of an oceanographic satellite equipped with a scatterometer [15]. This multiantenna fan-beam Doppler scatterometer was the first to be used for wind observations. Like the ERS-1/2 scatterometer [16], the NASA scatterometer (NSCAT) [17], and the advanced scatterometer (ASCAT) [18], several subsequent instruments have utilized fan-beam antennas and either doppler filters or range gating. The first space-borne scatterometer to use a dual rotating-beam was the sea wind scatterometer [19], which was followed by the Indian Oceansat-2 scatterometer [20]. Other applications of the scattering measures from these sensors include sea ice type mapping, iceberg identification, and soil moisture and vegetation density assessment [21]. Also, future scatterometers with improved resolution and dual-frequency capability have been proposed by [22]. To increase the accuracy of soil moisture measurements, the soil moisture active passive (SMAP) mission, which was scheduled to launch in 2014-15, will use a low-resolution L band scatterometer in conjunction with an L band radiometer [23].

1.5 Motivation

At present, radar remote sensing has become a very essential and dependable technology for studying the Earth and monitoring the natural changes caused by various ecological and anthropogenic factors. The majority of active remote sensing radar systems use fixed frequency bands i.e., X, C, S, L, and P bands, which are approximately 10, 6, 3, 2, and 0.5 GHz, respectively. The radar system parameters are the frequencies, antenna gain, polarization, receiver, and transmitter angle (i.e., zenith and azimuth angle). These parameters can be optimized to find the best radar system parameter for a wide range of applications in the scientific field of remote sensing. The distinctive features of the microwave region, such as its ability to penetrate the cloud, to some extent rain, vegetation, upper soil surface, and the fact that it has its own energy source and can therefore collect day-night information, are extremely promising compared to optical sensors. The penetration depth depends on

the wavelength used, polarization, vegetation type, soil moisture, and soil particle compositions. The higher frequencies, such as the X and C bands, have less penetrating power and thus can be used for vegetation and forest information. However, low frequencies of electromagnetic signals (i.e., S, L, and P bands) can easily penetrate the soil surface underlying vegetation and forest. Therefore, S, L, and P bands are specifically used to gather land surface parameter information.

The term "imaging radar" refers to a collective term comprising airborne and space-borne radar systems. In imaging radar, an antenna is either attached to the underside of the aircraft or directed to the side. Consequently, this classification of devices was at first referred to as Side-Looking Radar (SLR) or Side-Looking Airborne Radar (SLAR). Nevertheless, modern radar technology is known as SAR, and it makes use of sophisticated techniques for data processing. The imaging radar system generates continuous strips of imagery representing high-resolution views of ground areas parallel to the platform's flight line. In the past few decades, some prominent examples of the numerous measurement campaigns that used advanced air- and space-borne synthetic-aperture radar (SAR) systems, for instance, ERS-1/2, JERS-1, RADARSAT 1/2, and ENVISAT, etc., were achieved, and detailed list is tabulated in [7]. These campaigns were carried out better to understand the Earth's surface and atmosphere. These SAR systems give coherent radar images at various frequencies and polarizations, and they also have different frequency ranges. Many remote sensing tasks, such as monitoring sea and ice, land classification, soil moisture monitoring, surface roughness estimation, and forest/crop biomass evaluation, have been successfully completed by statically analyzing the collected data and utilizing physics-based inversion algorithms [24–26]. In addition, throughout the previous two decades, a variety of advanced techniques have been developed and applied to the SAR data. The technologies, such as interferometry [27, 28], SAR polarimetry [29, 30], and tomography [31], lead to noteworthy results in Earth remote sensing.

The majority of sensor technology problems for specialized applications, such as measuring high-precision data and monitoring land surface, vegetation, forest, ice, and ocean, relied primarily on monostatic geometry till now. However, very few bistatic observable quantities were reported after the European Space Agency (ESA) supported the concept of bistatic/companion satellites for different scientific objectives in the field of the cryosphere, biosphere, and solid earth research [32]. In addition, the majority of the early demonstration of bistatic observable quantities for remote sensing applications was conducted using towers, followed by aircraft, stratospheric balloons, and low earth orbits through Global Navigation Satellite System- Reflectometry (GNSS-R) techniques [33]. The concept of companion satellites to existing sensors such as HARMONY(two companion satellites following one of ESA's Copernicus Sentinel-1 satellites), TerraSAR-X, GNSS-R, and SAOCOM satellite is proposed for a cost-effective solution of bistatic/multistatic geometry [32, 34–36]. Consequently, it is still crucial to obtain experience and knowledge of bistatic remote sensing techniques.

Indoor and outdoor experimental measurements at low altitudes (i.e., ground and aircraft level) play a significant role in investigating and implementing new remote sensing methods. It is also valuable for validating surface and volume scattering models. In the last 50 years, numerous experimental investigations have been reported to understand the insights of the backscattered electromagnetic signal from vegetated lands, rough bare surfaces, forests, etc.. The experimental finding-based study helps validate and improve the theoretical scattering models to provide efficient and accurate information on the land-biogeophysical parameters such as soil moisture, roughness parameter, leaf area index, vegetation water content, and plant height. On the other hand, the experimental results are also used to develop the empirical and semi-empirical models, namely Oh model [37], Dubois model [38], and Integral Equation Model (IEM) [39] model for soil surface information retrieval. Compared to backscattering, very few bistatic experiments

have been performed in the forward scattering alignment convention. Stephen T. Cost [40] of Ohio State University performed the first experimental bistatic measurement in 1965. The experimental work measures natural terrains' normalized bistatic scattering coefficient such as sand, loam, dry grass, and soybeans over a wide range of bistatic angles and antenna polarizations at the X band. The Applied Electronics Laboratories, Stanmore, Middlesex, UK, performed the first airborne bistatic reflection of land and sea in 1967 [41]. A continuous wave with the transmitter and receiver installed on different aircraft measured X band scattering echos. The land cover under investigation includes open grassland, trees, and buildings. However, there is considerably little documentation about the conditions during the studies, especially for the sea clutter experiments. In recent times, more bistatic indoor experimental evaluations of rough surfaces have been carried out in two separate labs. The first one was accomplished by Roger De Roo (Michigan University) [42], where several rough surfaces with constant moisture in the soil were tested at X band and validated to different surface scattering models. In the second experiment, which was carried out at the experimental Microwave Signature Laboratory (EMSL), three distinct rough surfaces with a consistent soil moisture level were subjected to measurements at different frequencies and validated against a variety of scattering models [43]. The third experiment which is carried out in the remote sensing laboratory of the Department of Physics, IIT(BHU), India. The experimental techniques of two horn antennae bistatic scatterometer system for X, C, and L bands were developed to evaluate the capability of the bistatic radar system in a specular plane for monitoring/retrieving land bio-geophysical parameters such as Leaf area index, vegetation water content, and soil moisture, as well as their validation by developing or modifying a bistatic scattering model. [44, 45].

As a result, we may conclude that

✓There is a lack of experimental investigation on the fully polarimetric bistatic scattering phenomenon for different targets such as forests, wetlands, oceans, vegetation, and bare land surfaces.

✓The lack of robust methodological challenges (including physical, semi-empirical, and empirical model development) that allow consideration of experimental bistatic radar returns at ground and aircraft altitude.

1.6 Research objective

In view of the above motivation, the objectives of this thesis are as follows:

✓To design and explore the dual/fully-polarimetric bistatic scatterometer system over a wide range of specular incidence angles (from 20° to 60°) in the forward scattering alignment convention.

✓Examining the bistatic scattering phenomenon for rough vegetated lands.

✓Optimization of bistatic radar returns from rough vegetated lands at different frequencies, polarization, and specular incidence angle to determine the best bistatic geometric configurations.

✓To find limitations and advantages of bistatic scatterometer measurements techniques

✓Investigate the robust methodological challenges, including physical, semi-empirical, and empirical models that consider experimental bistatic radar returns at ground altitude.

✓Interpretation of the total bistatic scattering decomposition using the first-order radiative transfer model that provides insights into microwave interaction with the temporal change in the vegetated fields, namely, rice and wheat crops.

✓To develop a model inversion approach for land bio-geophysical parameters, such as soil moisture, leaf area index, fresh biomass, vegetation water content, and plant height, retrievals using a first-order radiative transfer model.

✓To investigate the potential of the machine learning techniques, specifically the SVR model using three different kernels, i.e., radial, polynomial and linear, for land-biogeophysical parameters information retrieval.

1.7 Thesis outline

The subject matter of the thesis is organized in the following eight chapters:

Chapter 1 gives an overview of the background and concepts of remote sensing, as well as microwaves for remote sensing. It also highlights the motivation of this research and its objectives.

Chapter 2 describes the detailed investigation of the literature available for the surface, the volume scattering model, and the scatterometer system. In addition, this chapter also emphasizes the land and vegetation parameters used in our study. This chapter also addresses the state-of-the-art.

Chapter 3 discusses the types of radar configurations, radar coordinate systems, how radar equation can be used to capture the fully polarimetric scattering response of the distributive targets, and the advantages/disadvantages of the bistatic radar system.

In Chapter 4, far-field co-polarized (i.e., HH and VV) bistatic specular scattering measurements were carried out for rice crops using a bistatic scatterometer system over a wide specular incidence angle (i.e., from 20° to 60° at an interval of 10°) for X and C bands. A correlation analysis was employed to find optimum radar wave parameters of interest, such as specular incidence angle, polarization, and frequency for vegetation biophysical parameter monitoring. A parameterized modified radiative transfer model was used to simulate the bistatic scattering from vegetation and retrieve vegetation biophysical parameters.

In Chapter 5, the bistatic microwave scattering model based on the coherent and incoherent theory for rough vegetated land (i.e., wheat crop overlaying rough soil surface)

at X and L bands were developed. The scattering model also facilitates the retrieval of vegetation biophysical (i.e., leaf area index) and land surface parameter (i.e., soil moisture) information. The simulation values of the bistatic scattering coefficients from the model are validated against the measured value of the bistatic scatterometer system.

In Chapter 6, the fully polarimetric (i.e., HH, VV, HV, and VH) bistatic scattering measurement from vegetation overlaying rough soil surface was carried out using an indigenous design bistatic scatterometer system for the C band. A comprehensive modified first-order radiative transfer model was developed to provide insight into microwave interaction with the temporal change in the vegetation and land surface parameters.

In Chapter 7, the potential of machine learning algorithms (i.e., support vector regression) was evaluated for the vegetation biophysical parameter retrieval using the dual-polarized (i.e., HH and VV) bistatic scatterometer measured data for the X and C bands.

Finally, Chapter 8 concludes the present thesis with a discussion of its implications and future prospects.

****